



Galactic Cosmic-Rays in a Breeze

Gwenael Giacinti^a, Andrew M. Taylor^b^a*Max-Planck-Institut für Kernphysik, Postfach 103980, 69029 Heidelberg, Germany*^b*Dublin Institute for Advanced Studies, 31 Fitzwilliam Place, Dublin 2, Ireland*

Abstract

We study a scenario in which the Fermi bubbles are formed through a Galactocentric outflow of gas and pre-accelerated cosmic-rays (CR). We take into account CR energy losses due to proton-proton interactions with the gas present in the bubbles, and calculate the associated gamma-ray emission. We find that CRs diffusing and advecting within a breeze outflow result in an approximately flat surface brightness profile of the gamma-ray emission, as observed by Fermi satellite. Finally, we apply similar outflow profiles to larger Galactocentric radii, and investigate their effects on the CR spectrum and boron-to-carbon ratio. Hardenings can appear in the spectrum, even in cases with equal CR diffusion coefficients in the disk and halo [1].

Keywords: cosmic rays, galactic wind, Fermi bubbles

1. Introduction

A number of indications that the center of our Galaxy feeds a wind has been found over the last few decades. This body of evidence has been provided from observations in a broad energy range: radio HI [2], infrared (IR) [3], and X-rays [4]. IR observations have also indicated that this wind continues further away [5], and that it may be responsible for the larger structures observed out of the Galactic plane. Absorption line features in the spectra of Active Galactic Nuclei (AGN) can be used as a probe of the structure of the gas flow: See Reference [6], whose results indicate the presence of a coherent gas flow, consistent with an outflow being directed away from the Galactic plane.

More recent gamma-ray and radio observations have shown the presence of extended non-thermal particle populations in bubble-like structures in the halo, both above and below the Galactic center (GC), see References [7, 8, 9, 10]. The current picture seems to indicate that cosmic-rays (CR) and hot gas are conveyed out from the GC region into the halo within a Galactocentric outflow.

As for the velocity of this outflow, values of ~ 300 km/s have been suggested in the region close to the Galactic disk (within \sim a couple of kiloparsecs), from the weakness of the X-ray features associated with the edge of the bubbles [7, 11, 12, 13]. At distances ~ 4 kpc and ~ 9 kpc away of the Galactic plane, observations of high velocity clouds suggest velocities of about ~ 150 km/s, cf. Reference [6]. Further out, towards the edges, velocities are $\lesssim 100$ km/s. In radio [10], the bending observed in the outflow at high latitudes may be related to the motion of our Galaxy towards Andromeda (relative velocity ~ 50 km/s).

In the present work, we study the secondary signatures produced by CRs embedded in outflows.

In Section 2, we focus on the Fermi bubbles. We then apply, in Section 3, a similar outflow velocity profile at larger Galactocentric radii, and investigate the possible traces it would leave on local CR observables, should such an outflow exist locally. We present our conclusions in Section 4.

2. Fermi bubbles: CRs and gamma-rays associated with a Galactocentric Outflow

A description for the propagation of cosmic rays in a turbulent region in which an advective flow is present is provided by,

$$\frac{\partial \psi_{\text{CR}}}{\partial t} = \nabla \cdot (\mathcal{D} \nabla \psi_{\text{CR}} - \mathbf{V} \psi_{\text{CR}}) + \frac{\partial}{\partial p} \left[\frac{p}{3} (\nabla \cdot \mathbf{V}) \psi_{\text{CR}} \right] - \frac{\psi_{\text{CR}}}{\tau_{\text{CR}}} + \mathcal{Q}_{\text{CR}}, \quad (1)$$

where $\psi_{\text{CR}}(\mathbf{r}, p, t)$ denotes the CR density per unit of particle momentum p , at spatial position r . Here \mathcal{Q}_{CR} is the cosmic-ray source term, \mathcal{D} is the cosmic-ray diffusion coefficient, and τ_{CR} is the cosmic-ray lifetime in the system.

For the advective flow of the gas, as motivated by observations, a divergence free velocity field is adopted, of the form

$$\mathbf{V} \cdot \hat{\mathbf{z}} = v_0 \times \frac{2 e^{\frac{1}{2}(1-\frac{d}{z})}}{1+z/d}, \quad (2)$$

where $v_0 = 300 \text{ km s}^{-1}$, $d = 1 \text{ kpc}$, and z is the distance to the Galactic plane. This profile broadly encapsulates the velocity profile of a “breeze” solution for the isothermal outflow problem [15, 16].

With regards the energy source driving this outflow, both a past AGN outburst event (see e.g. [17, 18, 19]), and a starburst phase or a sustained outflow driven by star formation in the Galactic centre (e.g. [20]) have been previously proposed. However, reference [21] claims that the present velocity data are not conclusive on the type of source responsible for this outflow. Energetically, the starburst-driven outflow luminosity is estimated to be $\approx (1-3) \times 10^{40} \text{ erg s}^{-1}$ [20]. The present level of AGN activity from the GC (of Sgr A*) is considerably below this ($L_{\text{Sgr A}^*} \sim 10^{33} \text{ erg s}^{-1}$), but there is a growing body of evidence that its level in the recent past was significantly higher [22, 23]. It therefore currently seems plausible for either energy source to be driving the outflow. We here choose to keep the discussion general, adopting instead the velocity profile of Eq. (2) as the starting point in our calculations.

We adopt a Monte Carlo approach to solve Eq. (1). Our results with this technique have been compared with those obtained using an explicit differential equation solver. We found excellent agreement in all cases.

We assume that the source term \mathcal{Q}_{CR} is located at the GC region and constant in time. The copresence of the resultant accumulated CRs with the ambient gas gives rise to gamma-ray bubble emission through π^0 production generated in proton-proton interactions. This emission may potentially account for the observed gamma-rays from the bubbles, as has previously been proposed by other authors [24].

We determine the level of this emission by convolving the accumulated CR density throughout the outflow region with the target gas density in the outflow. As motivated on theoretical [25], and observational [12] grounds, we adopt a constant gas density within the bubbles at the level $3 \times 10^{-3} \text{ cm}^{-3}$. In Fig. 1, we show a gamma-ray density map and a comparison of the gamma-ray bubble-edge profile with Fermi measurement. For these calculations, we took a CR luminosity of 10^{40} erg/s for the central source. In Fig. 1 (right panel), the origin of the diffuse gamma-ray emission in the $\theta > 0$ region is assumed purely galactic in origin. Should some component of the emission from this region be extragalactic, a reduction of the GC luminosity or bubble gas density would be required in order to account for such a reduction in required γ -ray emission intensity.

As can be seen in Fig. 1, a flat surface brightness profile for the bubbles is obtained when assuming that the velocity profile in the bubbles is described by Eq. (2). We note, however, that in reality a range of velocity profiles can provide such a uniform brightness, see for example [26]. In general, we find that for the case of a constant density ambient gas description, the current gamma-ray data can be said to prefer decelerating profiles. For decreasing gas density profiles, a sharper fall-off in the velocity profile, than that used in Eq. (2), would be required.

Although the cutoff at the edge of the bubbles is not well described by the simple constant density gas model (see red dashed line in Fig. 1), a steeper cutoff in the γ -ray profile can be achieved by an abrupt change in the gas density at the bubble edge (see red solid line), as motivated in certain models [20]. Another motivation for such an origin for the bubble edges comes from a comparison of their morphology as seen in gamma-rays [7] and in radio [10]. If GeV protons (resp. electrons) give rise to the γ -ray (resp. radio) emission, it would be surprising that the electrons extend out to larger latitudes than the protons. Such a difference between the morphologies of the γ -ray and radio data dis-

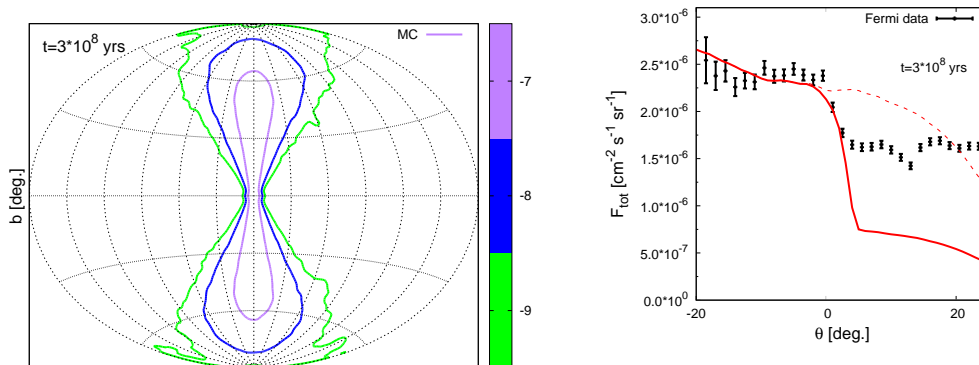


Figure 1: *Left panel:* Contours showing the \log_{10} of the gamma-ray flux surface brightness (in $\text{cm}^{-2} \text{s}^{-1} \text{sr}^{-1}$) from the bubbles, following CR interaction with the gas in the outflow. The different line colours indicate the corresponding contour values, cf. values in the colour bar. *Right panel:* Comparison of the edge of the (1 – 2) GeV gamma-ray bubble from our model with that from the Fermi observation analysis. We count the angle θ from the edge of the bubble. At large θ , for the energy bin considered, further diffuse gamma-ray background [14] dominates the observed flux —the model values sit below this level in this region. Solid line for a decrease in the gas density at the bubble edge, and dashed line for a constant density throughout.

favours simple leptonic scenarios for the γ -ray bubbles. However, despite these challenges, more involved diffuse acceleration models supporting a scenario in which both the radio and gamma-ray emission are leptonic in origin are currently viable [27].

One simple explanation for the difference in the latitudinal profiles of the radio and gamma-ray emissions is that both protons and electrons possess extended distributions, and that the difference in morphology of their secondary emissions is due to differing distributions of target gas and magnetic fields. A potential association of IceCube high energy neutrinos [28], with the bubbles and beyond [29], allows such a hadronic origin scenario for the gamma-rays to be tested in the near future.

With regards the parameter d , which dictates the turnover distance in the outflow velocity profile described by Eq. (2), a comparison of the fits to the radial gamma-ray profile of the Fermi bubbles is provided in Fig. 2, through a consideration of the $\chi_{\text{d.o.f.}}^2$ contours. The upper plot in this figure shows that for the majority of the parameter space, small values of d are problematic, with the large $\chi_{\text{d.o.f.}}^2$ values obtained reflecting the fact that such values lead to centrally brightened profiles, incompatible with the flat profile suggested by the data. However, the middle and lower panels show that the results for such intermediate and “large” values of d both show considerable regions of parameter space able to provide sufficiently flat profiles in agreement with that measured.

3. Local Outflow and CR Fluxes at Earth

In this Section, we study the impact that an outflow at larger Galactocentric radii would have on CR observables in the disk. The impacts of winds with either constant velocities [30, 31, 32] or velocities $V(z)$ increasing with height z in the halo [33, 34, 35, 36] have already been studied extensively in the literature. In the present work, we decide instead to study the case of outflows whose dV/dz become negative above a given height z_{max} . As far as we know, such a case has not been studied yet, with the exception of Reference [1]. We note that such velocity profiles do not correspond to those expected for winds driven by cosmic-rays. For such winds, $dV/dz \geq 0$ at all z , see Refs. [37, 38, 39, 40, 41, 42, 43, 36], as well as the numerical simulations of Refs. [44, 45, 46, 47]. However, the case of an outflow decelerating in the halo is worth studying for, at least, two reasons. First, some studies have argued that some galaxies may fail to produce “successful”, accelerating winds with a positive dV/dz at all heights in the halo, for instance because of ram pressure from infalling material: See e.g. Reference [48]. Second, such a profile is preferred for the Fermi bubbles, as argued in the previous Section. It is unclear at the present time whether a breeze profile may apply to larger Galactocentric radii or not. Therefore, it is interesting to provide possible signatures that could confirm or rule out such a scenario.

As a first approximation, we assume in the fol-

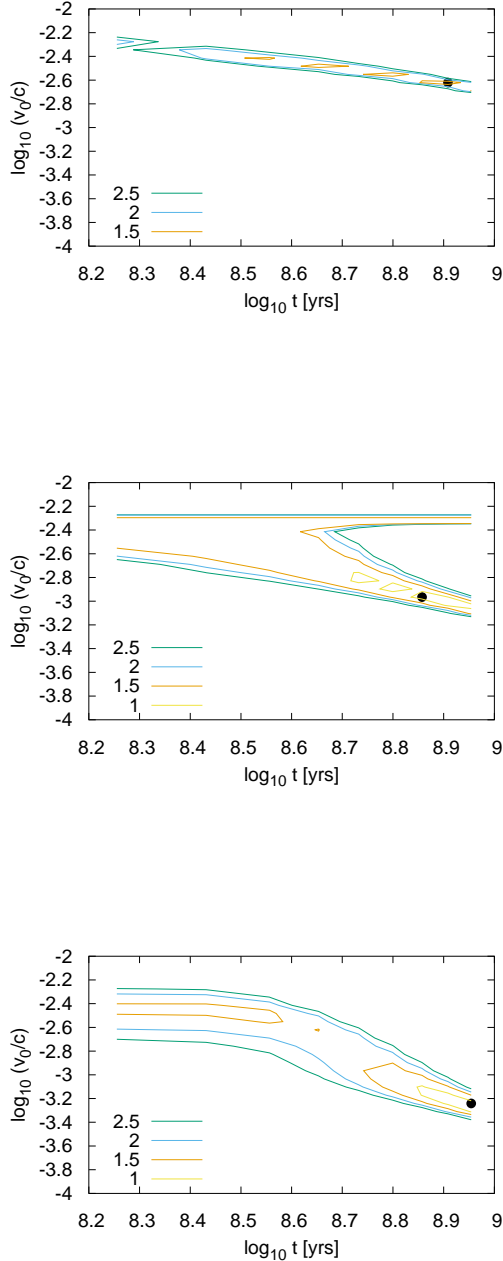


Figure 2: Plots showing $\chi^2_{\text{d.o.f.}}$ contours for fits to the γ -ray flux surface brightness profile of the Fermi-bubbles using Fermi satellite measurements in the range $\theta < 2[\text{deg.}]$. The different contour plots cover a range of different cases for the distance d , over the range: $d = 0.3 \text{ kpc}$ (top); $d = 1 \text{ kpc}$ (middle); $d = 2 \text{ kpc}$ (bottom). In each plot, the position of the best-fit parameters is marked with a black circle.

lowing that variations of CR propagation or source parameters along the direction of the galactocentric radius can be ignored. We then assume that V only depends on z . We wrote a code which solves numerically Equation (1) in planar 1D, for any arbitrary profiles of $V(z)$ and $\mathcal{D}(z, E)$. This code was presented and tested in [1]. In particular, we checked that it reproduces correctly the expected CR density profiles in the halo for the known cases of $V = \text{constant}$ [30] and $V(z) \propto z$ [35], which are respectively constant and decreasing with z . On the contrary, the profiles $V(z)$ we consider below result in an increase of CR density above z_{max} . Hereafter, we set $\psi_{\text{CR}} = 0$ at $z = H$ as a boundary condition, where H denotes the size of the halo. The CR density then decreases again when $z \rightarrow H$, due to CR escape. Such boundary conditions are widely used in Galactic CR propagation codes, and may correspond to the height above which the magnetic field is too weak to confine cosmic-rays. We stress however that, in general, the use of such conditions is not guaranteed to be justified, and may not be a good proxy for the actual physical picture: For instance, if a strong wind is present up to large z , see e.g. Refs. [37, 43]. In the latter case, the effective “halo size” seen by GeV–PeV CRs corresponds instead to the (energy-dependent) height above which CR advection wins over CR diffusion. In the following, for our breeze profiles, $V(z)$ is small at large z , and we stick to the aforementioned boundary condition at $z = H$.

We calculate the steady-state distributions $\psi_{\text{CR}}(z, E)$ for CR protons, and $\psi_{\text{B,C}}(z, E)$ for boron and carbon nuclei. We calculate the production and destruction of boron as described in Ref. [1], and we use the cross-section values quoted there. For the density profile of the target gas, $n(z)$, we take: $n = 0.85 \text{ cm}^{-3}$ at $|z| \leq h$, and 10^{-3} cm^{-3} otherwise. The source term \mathcal{Q}_A for primary nuclei A is set to:

$$\mathcal{Q}_A = \begin{cases} \mathcal{F}_A \mathcal{Q}_{\text{CR}} & , \text{ at } |z| \leq h \text{ (disk)} \\ 0 & , \text{ at } h < |z| \leq H \text{ (halo)} \end{cases} \quad (3)$$

where \mathcal{F}_A denotes the fraction of nuclei A emitted at the sources. The disk width is set to $h = 200 \text{ pc}$. For clarity, we assume below that there are no sources of primary boron. See e.g. [32] for a non-zero \mathcal{Q}_{B} . We will not study here the hypothetical case where CR trapping around their sources contributes significantly to the boron-to-carbon ratio, e.g. [49]. In such a scenario, this ratio would contain little information on CR propagation on large scales in our Galaxy, and hence little constraints on

a local outflow. For clarity, we assume below that \mathcal{D} does not depend on z . We express it as:

$$\mathcal{D}(E/Z) = \mathcal{D}_{3\text{GV}} \left(\frac{E/Z}{3\text{GV}} \right)^\delta, \quad (4)$$

for nuclei of charge Z . We set $\delta = 0.44$ and $\mathcal{D}_{3\text{GV}} = 2.8 \times 10^{28} \text{ cm}^2 \text{ s}^{-1}$, which correspond to the best fit values of Ref. [32] for $H = 4 \text{ kpc}$. Ref. [50] also suggested the same value for δ . We verified that our code reproduces the expected boron-to-carbon ratios both for the cases of “no wind”, and “wind velocity constant with z ”.

In the static regime ($V = 0$), the boron current in the halo is $\mathcal{J}_{\text{B,Halo}} = -\mathcal{D}_{\text{B}} \partial \psi_{\text{B}} / \partial z \simeq \mathcal{D}_{\text{B}} \psi_{\text{B},0} / H$ ($h \ll H$). Therefore, in the static regime, the boron-to-carbon ratio is

$$\frac{\psi_{\text{B},0}}{\psi_{\text{C},0}} \simeq \frac{\sigma_{\rightarrow\text{B}}}{\sigma_{\text{B}\rightarrow} + \frac{\mathcal{D}_{\text{B}}(E)}{cn_0 h H}} = \frac{\tau_{\rightarrow\text{B},0}^{-1}}{\tau_{\text{B}\rightarrow,0}^{-1} + \frac{\mathcal{D}_{\text{B}}(E)}{hH}}, \quad (5)$$

where indices “0” mean “at $z = 0$ ”, and $\sigma_{\rightarrow\text{B},\text{B}\rightarrow} = 1/cn\tau_{\rightarrow\text{B},\text{B}\rightarrow}$ are the production and destruction cross-sections for boron. With the parameter values we take here, the diffusion term “ $\frac{\mathcal{D}_{\text{B}}(E)}{hH}$ ” dominates over the “ τ ” term only around the last couple of points in the AMS-02 data [51], which is why the slope in the data, at \lesssim a few $\times 100 \text{ GeV/nucleon}$, looks flatter than 0.44. This calls for a better knowledge of cross-sections, as also noted by [32].

In the hypothetical case of a wind with a velocity constant with z , the “ $\frac{\mathcal{D}_{\text{B}}(E)}{hH}$ ” term in Eq. (5) must be replaced with “ $V/(1 - \exp[-HV/\mathcal{D}_{\text{B}}(E)])h$ ”, cf. Ref. [32]. Let us denote $z_* = \mathcal{D}/V$, the distance beyond which advection dominates over diffusion. In this particular setup, low-energy CRs with $z_* = \mathcal{D}/V < H$ advect to the boundary, whereas higher-energy CRs diffuse to the boundary. This introduces a flattening in the boron-to-carbon ratio at low energies ($z_* \propto E^\delta$ for $V = \text{constant}$). A value of V larger than a few tens of km/s for $H \sim 10 \text{ kpc}$ is incompatible with the data. This excludes a strong “ $V = \text{constant}$ ” wind. However, the current boron-to-carbon data does *not* exclude the presence of a strong wind in general, as other wind profiles with $V \neq \text{constant}$, such as $V(z) \propto z$, are allowed by the data. For winds with $V(z) \propto z$, $z_* \propto \sqrt{\mathcal{D}}$. For a CR spectrum at the sources $\propto E^{-\alpha}$, the slope of the CR flux at Earth then tends to $-\alpha - \delta/2$, cf. Reference [35].

From now on, we focus on $V(z)$ profiles that decrease above a height z_{max} in the halo. In Figure 3,

we show eight profiles (lower panel) and their impact on the CR spectrum (upper panel) and boron-to-carbon ratio (middle panel) at $z = 0$. For reference, we also plot results for the “benchmark fit” of [32] for $V = 0$ (thin black line). The boron-to-carbon ratio measurements from AMS-02 experiment coincide with this line. Our goal here is *not* to provide a fit of the data. Instead, we take “caricatural” examples of $V(z)$ profiles with rather extreme parameter values, so as to make the impact of these parameters more visible. In some cases, changing the values of some of the parameters would provide a reasonable fit to the data.

We set the CR spectral index at the sources to $\alpha = 2.26$. We do not vary α , δ , $\mathcal{D}_{3\text{GV}}$, $n(z)$ or h , so as to help the reader distinguish between the contributions from the different wind parameters. For all eight profiles, $V = 0$ at $z \leq z_{\text{min}}$, then increases $\propto z$ up to V_{max} at $z = z_{\text{max}}$, and then decreases on a typical length scale d' :

$$V(z) = \begin{cases} 0 & , \text{ at } |z| \leq z_{\text{min}} \\ \frac{V_{\text{max}}(z - z_{\text{min}})}{z_{\text{max}} - z_{\text{min}}} & , z_{\text{min}} < |z| \leq z_{\text{max}} \\ \frac{V_{\text{max}}}{1 + (z - z_{\text{max}})/d'} & , z_{\text{max}} < |z| \leq H \end{cases} \quad (6)$$

Each of these scenarios is represented by the same line type and colour in each panel of Fig. 3. Let us denote by A (resp. B) the thick (resp. thin) red solid lines in Fig. 3, C (resp. D) the thick (resp. thin) green dashed lines, E (resp. F) the thick (resp. thin) magenta dotted lines, and G (resp. H) the dark (resp. light) blue dashed-dotted lines. We take $z_{\text{min}} = 200 \text{ pc}$ for $\{A, B, C, D\}$, and 2 kpc otherwise. $z_{\text{max}} = 1 \text{ kpc}$ for $\{A, B, C, D\}$, 2.8 kpc for $\{E, F\}$, and 10 kpc for $\{G, H\}$. $V_{\text{max}} = 60 \text{ km/s}$ for $\{A, B\}$, and 600 km/s otherwise. $d' = 2 \text{ kpc}$ for $\{A, C, E\}$, 5 kpc for H, and 20 kpc otherwise. $H = 5 \text{ kpc}$ for $\{A, C, E\}$, and 50 kpc otherwise.

In all cases, when the CR energy is sufficiently high for diffusion to win over advection at all z , the problem simplifies to a basic leaky-box with homogeneous diffusion coefficient. Spectra (upper panel) then all tend to $\propto E^{-\alpha - \delta} = E^{-2.7}$, e.g. above $\sim 100 \text{ GeV}$ (resp. $\sim 10 \text{ PeV}$) for A (resp. G). Case A shows that a weak outflow with such a profile introduces a turnover in the CR spectrum at low energies. This might explain the turnover measured below $\sim 10 \text{ GeV}$ from molecular clouds. The outflow reduces the “box” (in which low-energy CRs diffuse and can come back to $z = 0$) to an effective size $z_* \ll H$, where $z_*(E)$ is the height where advection wins over diffusion. For these low-energy

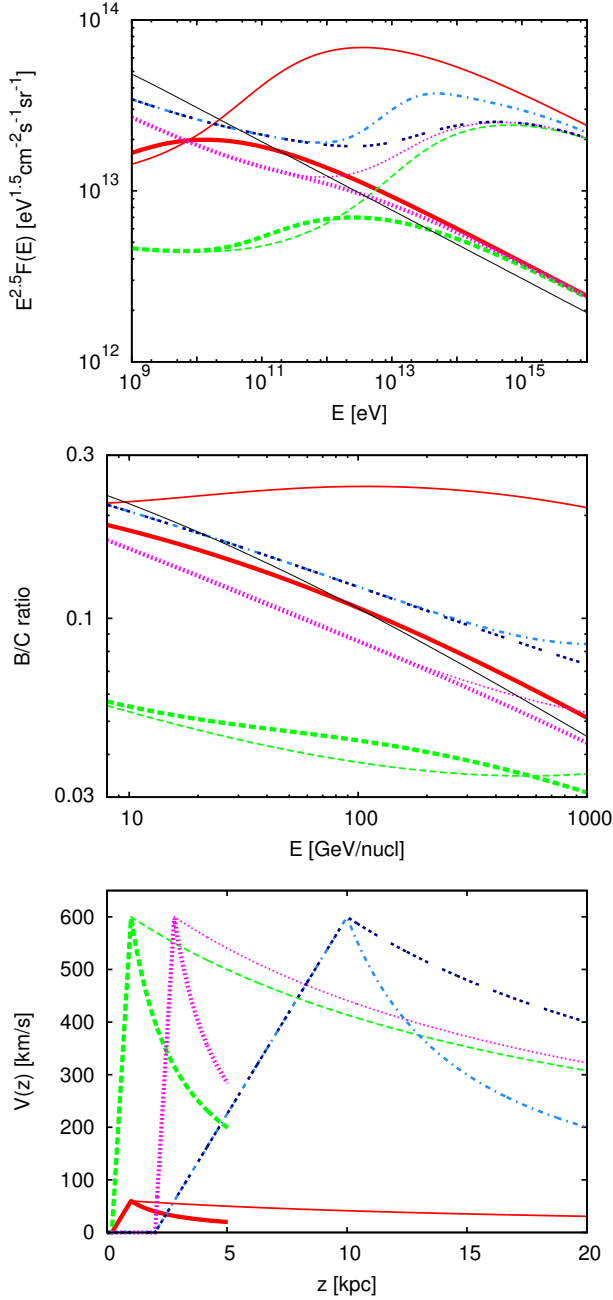


Figure 3: CR flux (*upper panel*) and B/C ratio (*middle panel*) at $z = 0$, for the outflow profiles displayed in the *lower panel* ($20 \text{ kpc} < z \leq 50 \text{ kpc}$ not shown). We do *not* try to fit the data. $\mathcal{D}_{3 \text{ GV}} = 2.8 \times 10^{28} \text{ cm}^2 \text{ s}^{-1}$, $\delta = 0.44$, $h = 200 \text{ pc}$, $H = 5$ or 50 kpc (see end of lines on the right panel), $n(z) = 0.85 \text{ cm}^{-3}$ for $|z| \leq h$ and 10^{-3} cm^{-3} otherwise, CR spectrum at sources $\propto E^{-2.26}$, and total power injected in CRs at $|z| \leq h$ in this region of the disk set to $\approx 3.3 \times 10^{39} \text{ erg pc}^{-2} \text{ yr}^{-1}$. Each scenario is represented by the same line type on each panel, see text. Thin black line for $V = 0$, $H = 4 \text{ kpc}$, and other parameters unchanged.

CRs, advection dominates in the region of large V around $z = z_{\text{max}}$. This region then acts as a bottleneck for them. A small turnover also occurs in the boron-to-carbon ratio. When increasing the extent of the wind, and then the size Δz of the region in the halo in which V is greater than a fraction of V_{max} , the turnover is shifted to higher energy: Indeed, in this case, a larger $\mathcal{D}(E)$ is required for diffusion to win over advection, see curves B. The CR flux at high energies in case B is ten times larger than in case A, because we kept $\mathcal{D}_{3 \text{ GV}}$ fixed in these examples, and did not rescale it with H .

Increasing V_{max} also increases the energy of the aforementioned feature, see C and D. More interestingly, CRs below this energy that can come back to $z = 0$, probe the part $\propto z$ of the wind, because $z_* \leq z_{\text{max}}$ for them. Since $z_{\text{max}} \gg z_{\text{min}} (\approx 0)$ in C and D, this results in a “ $V(z) \propto z$ ” scenario [35], and the CR spectrum (resp. boron-to-carbon ratio) slope tends to $-\alpha - \delta/2$ (resp. $-\delta/2$) at low energy, see green lines in Fig. 3. On the contrary, if one increases the altitude z_{min} of the launching of the wind, the CR spectrum (resp. boron-to-carbon ratio) slope tends to $-\alpha - \delta$ (resp. $-\delta$), as for the “ $V = 0$ ” scenario: See the magenta lines for the cases E and F. This is due to the fact that, at these low energies, $z_{\text{min}} \gg z_* - z_{\text{min}}$. Therefore, low-energy CRs see a small, energy-independent, effective leaky-box of height $\approx z_{\text{min}}$. In the cases E and F, $z_{\text{max}} - z_{\text{min}} \ll z_{\text{min}}$, and, with increasing CR energy, there is a “quick” transition to a bigger box of effective size $\approx H$: The slopes of the magenta CR spectra are $\approx -\alpha - \delta$ both at low and high energies in the energy range displayed in the upper panel.

For the case G, there is a hint of a smooth transition, at low energy, from a $\sim -\alpha - \delta$ to a $\approx -\alpha - \delta/2$ slope. Indeed, z_{min} has the same large value as in case F, but, for G, $z_{\text{max}} - z_{\text{min}}$ is not small compared to z_{min} . It is interesting to note that G and H are not far from fitting the existing experimental data for the boron-to-carbon ratio, despite having velocity profiles very different from the $V = 0$ profile of the “benchmark fit” (thin black line). The impact of d' on the CR spectrum is visible by comparing G with H. H, the profile with a faster fall off at high z , achieves the transition between the two limiting regimes in a smaller energy interval. A hardening (upturn) is also present in the boron-to-carbon ratio for the cases D, F, and H.

Green, magenta, and blue lines show a hardening in the CR spectrum around $\sim 10^{10-13} \text{ eV}$, due to the launching of a wind in the halo. For some

parameter values, it is possible to make it coincide better with the one measured at 200 GV in the CR spectra by PAMELA, CREAM and AMS-02 experiments. Thence, even in the limiting case of equal \mathcal{D} in the disk and in the halo, such a hardening may arise from the launching of a breeze or wind. This argument is valid for cases with $dV/dz > 0$ above z_{\max} too. As noted above, similar hardenings also appear in the boron-to-carbon ratio. This does not contradict the experimental data, provided that the hardening is concealed at higher energies, or remains within the systematics of the detectors. Regarding the second of these possibilities, conflicts in secondary to primary ratios have been reported in existing data sets, cf. Ti/Fe ratio by HEAO-3-C3 [52], ATIC-2 [53], and comparison to the boron-to-carbon ratio [51].

4. Conclusions and perspectives

We presented in Section 2 a hadronic model of the Fermi bubbles. Assuming that they result from a Galactocentric outflow carrying pre-accelerated cosmic-rays, we calculated the gamma-ray emission produced by the CRs interacting with the gas present in the bubbles. We showed that outflows decelerating with distance to the Galactic disk can reproduce the flat gamma-ray surface brightness of the bubbles, in accordance with the measurements from Fermi satellite. Our description for the outflow profile is enclosed in breeze solutions of isothermal winds.

Motivated by the above findings, we studied in Section 3 the impacts that similar types of outflow profiles would have on the CR spectra at Earth, should such outflows exist at larger Galactocentric radii. Competition between CR diffusion and advection in the halo can produce an inflection point in the CR spectrum at $z = 0$. A hardening can appear in the CR spectrum due to the launching of a wind or breeze in the halo, even in the hypothetical, limiting case of equal CR diffusion coefficients in the halo and disk.

Although a breeze outflow scenario is currently only motivated for the outflow from the GC region, we conclude from the above results that future observations should be able to test its presence or absence at larger radii, thanks to local CR observables.

Acknowledgments

AT acknowledges a Schroedinger fellowship at DIAS.

References

- [1] A. M. Taylor, G. Giacinti, Cosmic rays in a galactic breeze, *Phys. Rev. D* 95 (2) (2017) 023001. [arXiv:1607.08862](#), [doi:10.1103/PhysRevD.95.023001](#).
- [2] F. J. Lockman, The H I halo in the inner galaxy, *ApJ* 283 (1984) 90–97. [doi:10.1086/162277](#).
- [3] M. Morris, E. Serabyn, The Galactic Center Environment, *Annu. Rev. Astron. Astrophys.* 34 (1996) 645–702. [doi:10.1146/annurev.astro.34.1.645](#).
- [4] L. X. Cheng, M. Leventhal, D. M. Smith, W. R. Purcell, J. Tueller, A. Connors, D. Dixon, R. L. Kinzer, J. G. Skibo, A Maximum Entropy Map of the 511 keV Positron Annihilation Line Emission Distribution Near the Galactic Center, *ApJL* 481 (1997) L43–L46. [doi:10.1086/310638](#).
- [5] J. Bland-Hawthorn, M. Cohen, The Large-Scale Bipolar Wind in the Galactic Center, *ApJ* 582 (2003) 246–256. [arXiv:astro-ph/0208553](#), [doi:10.1086/344573](#).
- [6] B. A. Keeney, C. W. Danforth, J. T. Stocke, S. V. Penton, J. M. Shull, K. R. Sembach, Does the Milky Way Produce a Nuclear Galactic Wind?, *ApJ* 646 (2006) 951–964. [arXiv:astro-ph/0604323](#), [doi:10.1086/505128](#).
- [7] M. Su, T. R. Slatyer, D. P. Finkbeiner, Giant Gamma-ray Bubbles from Fermi-LAT: Active Galactic Nucleus Activity or Bipolar Galactic Wind?, *ApJ* 724 (2010) 1044–1082. [arXiv:1005.5480](#), [doi:10.1088/0004-637X/724/2/1044](#).
- [8] R.-z. Yang, F. Aharonian, R. Crocker, The Fermi bubbles revisited, *Astron. Astrophys.* 567 (2014) A19. [arXiv:1402.0403](#), [doi:10.1051/0004-6361/201423562](#).
- [9] M. Ackermann, A. Albert, W. B. Atwood, L. Baldini, J. Ballet, G. Barbiellini, D. Bastieri, R. Bellazzini, E. Bissaldi, R. D. Blandford, et al., The Spectrum and Morphology of the Fermi Bubbles, *ApJ* 793 (2014) 64. [arXiv:1407.7905](#), [doi:10.1088/0004-637X/793/1/64](#).
- [10] E. Carretti, R. M. Crocker, L. Staveley-Smith, M. Haverkorn, C. Purcell, B. M. Gaensler, G. Bernardi, M. J. Kesteven, S. Poppi, Giant magnetized outflows from the centre of the Milky Way, *Nature* 493 (2013) 66–69. [arXiv:1301.0512](#), [doi:10.1038/nature11734](#).
- [11] J. Kataoka, M. Tahara, T. Totani, Y. Sofue, L. Stawarz, Y. Takahashi, Y. Takeuchi, H. Tsunemi, M. Kimura, Y. Takei, C. C. Cheung, Y. Inoue, T. Nakamori, Suzaku Observations of the Diffuse X-Ray Emission across the Fermi Bubbles’ Edges, *ApJ* 779 (2013) 57. [arXiv:1310.3553](#), [doi:10.1088/0004-637X/779/1/57](#).
- [12] T. Fang, X. Jiang, High Resolution X-Ray Spectroscopy of the Local Hot Gas along the 3C 273 Sightline, *ApJL* 785 (2014) L24. [arXiv:1403.2028](#), [doi:10.1088/2041-8205/785/2/L24](#).
- [13] A. J. Fox, R. Bordoloi, B. D. Savage, F. J. Lockman, E. B. Jenkins, B. P. Wakker, J. Bland-Hawthorn, S. Hernandez, T.-S. Kim, R. A. Benjamin, D. V. Bowen, J. Tumlinson, Probing the Fermi Bubbles in Ultraviolet Absorption: A Spectroscopic Signature of the Milky Way’s Biconical Nuclear Outflow, *ApJL* 799 (2015) L7. [arXiv:1412.1480](#), [doi:10.1088/2041-8205/799/1/L7](#).

- [14] A. A. Abdo, M. Ackermann, M. Ajello, W. B. Atwood, L. Baldini, J. Ballet, G. Barbiellini, D. Bastieri, B. M. Baughman, K. Bechtol, Fermi LAT Collaboration, Spectrum of the Isotropic Diffuse Gamma-Ray Emission Derived from First-Year Fermi Large Area Telescope Data, *Physical Review Letters* 104 (10) (2010) 101101. [arXiv:1002.3603](#), [doi:10.1103/PhysRevLett.104.101101](#).
- [15] J. W. Chamberlain, On the Existence of Slow Solutions in Coronal Hydrodynamics., *ApJ* 141 (1965) 320. [doi:10.1086/148119](#).
- [16] E. N. Parker, Dynamical Properties of Stellar Coronas and Stellar Winds, IV. The Separate Existence of Subsonic and Supersonic Solutions., *ApJ* 141 (1965) 1463. [doi:10.1086/148235](#).
- [17] F. Guo, W. G. Mathews, The Fermi Bubbles. I. Possible Evidence for Recent AGN Jet Activity in the Galaxy, *ApJ* 756 (2012) 181. [arXiv:1103.0055](#), [doi:10.1088/0004-637X/756/2/181](#).
- [18] F. Guo, W. G. Mathews, G. Dobler, S. P. Oh, The Fermi Bubbles. II. The Potential Roles of Viscosity and Cosmic-Ray Diffusion in Jet Models, *ApJ* 756 (2012) 182. [arXiv:1110.0834](#), [doi:10.1088/0004-637X/756/2/182](#).
- [19] M. V. Barkov, V. Bosch-Ramon, Formation of large-scale magnetic structures associated with the Fermi bubbles, *Astron. Astrophys.* 565 (2014) A65. [arXiv:1311.6722](#), [doi:10.1051/0004-6361/201322743](#).
- [20] R. M. Crocker, G. V. Bicknell, A. M. Taylor, E. Carretti, A Unified Model of the Fermi Bubbles, Microwave Haze, and Polarized Radio Lobes: Reverse Shocks in the Galactic Center’s Giant Outflows, *ApJ* 808 (2015) 107. [arXiv:1412.7510](#), [doi:10.1088/0004-637X/808/2/107](#).
- [21] K. C. Sarkar, B. B. Nath, P. Sharma, Supernovae vs. AGN: Clues to the origin of Fermi Bubbles from OVIII/OVII line ratio, *ArXiv e-prints* [arXiv:1610.00719](#).
- [22] G. Ponti, R. Terrier, A. Goldwurm, G. Belanger, G. Trap, Discovery of a Superluminal Fe K Echo at the Galactic Center: The Glorious Past of Sgr A* Preserved by Molecular Clouds, *ApJ* 714 (2010) 732–747. [arXiv:1003.2001](#), [doi:10.1088/0004-637X/714/1/732](#).
- [23] R. Terrier, G. Ponti, G. Bélanger, A. Decourchelle, V. Tatischeff, A. Goldwurm, G. Trap, M. R. Morris, R. Warwick, Fading Hard X-ray Emission from the Galactic Center Molecular Cloud Sgr B2, *ApJ* 719 (2010) 143–150. [arXiv:1005.4807](#), [doi:10.1088/0004-637X/719/1/143](#).
- [24] R. M. Crocker, F. Aharonian, Fermi Bubbles: Giant, Multibillion-Year-Old Reservoirs of Galactic Center Cosmic Rays, *Physical Review Letters* 106 (10) (2011) 101102. [arXiv:1008.2658](#), [doi:10.1103/PhysRevLett.106.101102](#).
- [25] R. Feldmann, D. Hooper, N. Y. Gnedin, Circumgalactic Gas and the Isotropic Gamma-Ray Background, *ApJ* 763 (2013) 21. [arXiv:1205.0249](#), [doi:10.1088/0004-637X/763/1/21](#).
- [26] K. C. Sarkar, B. B. Nath, P. Sharma, Multiwavelength features of Fermi bubbles as signatures of a Galactic wind, *MNRAS* 453 (2015) 3827–3838. [arXiv:1505.03634](#), [doi:10.1093/mnras/stv1806](#).
- [27] P. Mertsch, S. Sarkar, Fermi Gamma-Ray “Bubbles” from Stochastic Acceleration of Electrons, *Physical Review Letters* 107 (9) (2011) 091101. [arXiv:1104.3585](#), [doi:10.1103/PhysRevLett.107.091101](#).
- [28] IceCube Collaboration, Evidence for High-Energy Extraterrestrial Neutrinos at the IceCube Detector, *Science* 342 (2013) 1242856. [arXiv:1311.5238](#), [doi:10.1126/science.1242856](#).
- [29] A. M. Taylor, S. Gabici, F. Aharonian, Galactic halo origin of the neutrinos detected by IceCube, *Phys. Rev. D* 89 (10) (2014) 103003. [arXiv:1403.3206](#), [doi:10.1103/PhysRevD.89.103003](#).
- [30] A. J. Owens, J. R. Jokipii, Cosmic rays in a dynamical halo. I - Age and matter traversal distributions and anisotropy for nuclei. II - Electrons, *ApJ* 215 (1977) 677–689. [doi:10.1086/155401](#).
- [31] F. C. Jones, The dynamical halo and the variation of cosmic-ray path length with energy, *ApJ* 229 (1979) 747–752. [doi:10.1086/157010](#).
- [32] Y. Genolini, A. Putze, P. Salati, P. D. Serpico, Theoretical uncertainties in extracting cosmic-ray diffusion parameters: the boron-to-carbon ratio, *Astron. Astrophys.* 580 (2015) A9. [arXiv:1504.03134](#), [doi:10.1051/0004-6361/201526344](#).
- [33] I. Lerche, R. Schlickeiser, On the transport and propagation of cosmic rays in galaxies. I - Solution of the steady-state transport equation for cosmic ray nucleons, momentum spectra and heating of the interstellar medium, *MNRAS* 201 (1982) 1041–1072. [doi:10.1093/mnras/201.4.1041](#).
- [34] V. A. Dogiel, The cosmic-ray halo - Insight from gamma rays and cosmic-ray observations, in: H. Bloemen (Ed.), *The Interstellar Disk-Halo Connection in Galaxies*, Vol. 144 of IAU Symposium, 1991, pp. 175–186.
- [35] J. B. G. M. Bloemen, V. A. Dogiel, V. L. Dorman, V. S. Ptuskin, Galactic diffusion and wind models of cosmic-ray transport. I - Insight from CR composition studies and gamma-ray observations, *Astron. Astrophys.* 267 (1993) 372–387.
- [36] S. Recchia, P. Blasi, G. Morlino, Cosmic ray driven Galactic winds, *MNRAS* 462 (2016) 4227–4239. [arXiv:1603.06746](#), [doi:10.1093/mnras/stw1966](#).
- [37] V. S. Ptuskin, H. J. Voelk, V. N. Zirakashvili, D. Breitschwerdt, Transport of relativistic nucleons in a galactic wind driven by cosmic rays., *Astron. Astrophys.* 321 (1997) 434–443.
- [38] D. Breitschwerdt, V. A. Dogiel, H. J. Völk, The gradient of diffuse gamma -ray emission in the Galaxy, *Astron. Astrophys.* 385 (2002) 216–238. [arXiv:astro-ph/0201345](#), [doi:10.1051/0004-6361:20020152](#).
- [39] A. Socrates, S. W. Davis, E. Ramirez-Ruiz, The Eddington Limit in Cosmic Rays: An Explanation for the Observed Faintness of Starbursting Galaxies, *ApJ* 687 (2008) 202–215. [arXiv:astro-ph/0609796](#), [doi:10.1086/590046](#).
- [40] J. E. Everett, E. G. Zweibel, R. A. Benjamin, D. McCammon, L. Rocks, J. S. Gallagher, III, The Milky Way’s Kiloparsec-Scale Wind: A Hybrid Cosmic-Ray and Thermally Driven Outflow, *ApJ* 674 (2008) 258–270. [arXiv:0710.3712](#), [doi:10.1086/524766](#).
- [41] S. Samui, K. Subramanian, R. Srianand, Cosmic ray driven outflows from high-redshift galaxies, *MNRAS* 402 (2010) 2778–2791. [arXiv:0909.3854](#), [doi:10.1111/j.1365-2966.2009.16099.x](#).
- [42] E. A. Dorfi, D. Breitschwerdt, Time-dependent galactic winds. I. Structure and evolution of galactic outflows accompanied by cosmic ray acceleration, *Astron. Astrophys.* 540 (2012) A77. [arXiv:1304.1311](#), [doi:10.1051/0004-6361/201219666](#).

- 10.1051/0004-6361/201118082.
- [43] V. N. Zirakashvili, Cosmic ray propagation and interactions in the Galaxy, Nuclear Physics B Proceedings Supplements 256 (2014) 101–106. [arXiv:1412.0863](#), [doi:10.1016/j.nuclphysbps.2014.10.012](#).
- [44] M. Hanasz, H. Lesch, T. Naab, A. Gawryszczak, K. Kowalik, D. Wóltański, Cosmic Rays Can Drive Strong Outflows from Gas-rich High-redshift Disk Galaxies, *ApJL* 777 (2013) L38. [arXiv:1310.3273](#), [doi:10.1088/2041-8205/777/2/L38](#).
- [45] T. Peters, P. Girichidis, A. Gatto, T. Naab, S. Walch, R. Wünsch, S. C. O. Glover, P. C. Clark, R. S. Klessen, C. Baczynski, Impact of Supernova and Cosmic-Ray Driving on the Surface Brightness of the Galactic Halo in Soft X-Rays, *ApJL* 813 (2015) L27. [arXiv:1510.06563](#), [doi:10.1088/2041-8205/813/2/L27](#).
- [46] P. Girichidis, T. Naab, S. Walch, M. Hanasz, M.-M. Mac Low, J. P. Ostriker, A. Gatto, T. Peters, R. Wünsch, S. C. O. Glover, R. S. Klessen, P. C. Clark, C. Baczynski, Launching Cosmic-Ray-driven Outflows from the Magnetized Interstellar Medium, *ApJL* 816 (2016) L19. [arXiv:1509.07247](#), [doi:10.3847/2041-8205/816/2/L19](#).
- [47] C. M. Simpson, R. Pakmor, F. Marinacci, C. Pfrommer, V. Springel, S. C. O. Glover, P. C. Clark, R. J. Smith, The Role of Cosmic-Ray Pressure in Accelerating Galactic Outflows, *ApJL* 827 (2016) L29. [arXiv:1606.02324](#), [doi:10.3847/2041-8205/827/2/L29](#).
- [48] Y. Dubois, R. Teyssier, On the onset of galactic winds in quiescent star forming galaxies, *Astron. Astrophys.* 477 (2008) 79–94. [arXiv:0707.3376](#), [doi:10.1051/0004-6361:20078326](#).
- [49] M. D’Angelo, P. Blasi, E. Amato, Grammage of cosmic rays around Galactic supernova remnants, *Phys. Rev. D* 94 (8) (2016) 083003. [arXiv:1512.05000](#), [doi:10.1103/PhysRevD.94.083003](#).
- [50] C. Evoli, H. Yan, Cosmic Ray Propagation in Galactic Turbulence, *ApJ* 782 (2014) 36. [arXiv:1310.5732](#), [doi:10.1088/0004-637X/782/1/36](#).
- [51] A. Collaboration, Precision Measurement of the Cosmic Ray Boron-to-Carbon Ratio with AMS, International Cosmic Ray Conference.
- [52] V. Vylet, J. C. Waddington, R. W. Binns, L. T. Garrard, H. M. Israel, J. Klarmann, M. Metzger, Energy Spectra Between 10 and Several Hundred GeV/Nucleon for Elements From $_{18}\text{Ar}$ to $_{23}\text{V}$: Results from HEAO-3, International Cosmic Ray Conference 3 (1990) 19.
- [53] V. I. Zatsepin, A. D. Panov, N. V. Sokolskaya, J. H. Adams, H. S. Ahn, G. L. Bashindzhagyan, J. Chang, M. Christl, A. R. Fazely, T. G. Guzik, J. B. Isbert, K. C. Kim, E. N. Kouznetsov, M. Panasyuk, E. S. Seo, J. Watts, J. P. Wefel, J. Wu, Energy dependence of Ti/Fe ratio in the Galactic cosmic rays measured by the ATIC-2 experiment, *Astronomy Letters* 35 (2009) 338–342. [arXiv:0905.0049](#), [doi:10.1134/S1063773709050089](#).